Reduction of the twisted bilayer graphene chiral Hamiltonian into a 2×2 matrix operator and physical origin of flat bands at magic angles

Gerardo G. Naumis,* Leonardo A. Navarro-Labastida, Enrique Aguilar-Méndez, and Abdiel Espinosa-Champo
Departamento de Sistemas Complejos, Instituto de Física, Universidad Nacional Autónoma de México (UNAM), Apdo. Postal 20-364, 01000, CDMX, México

(Received 18 February 2021; revised 14 April 2021; accepted 2 June 2021; published 14 June 2021)

The chiral Hamiltonian for twisted graphene bilayers is written as a 2×2 matrix operator by a renormalization of the Hamiltonian that takes into account the particle-hole symmetry. This results in an effective Hamiltonian written in terms of Pauli matrices with three contributions: a kinetic term, a confinement potential, and a non-Abelian gauge field. The action of the proposed renormalization maps zero-mode flat bands into ground states. On each graphene layer, modes near zero energy have an antibonding nature in a triangular lattice. This leads to a phase-frustration effect associated with massive degeneration and makes flat-band modes similar to confined modes observed in other bipartite lattices. At magic angles, it is shown that the intralayer frustration is exactly zero. Surprisingly, the proposed Hamiltonian renormalization suggests that flat bands at magic angles are akin to floppy-mode bands in flexible crystals or glasses, making an unexpected connection between rigidity topological theory and twisted two-dimensional superconductor systems.

DOI: 10.1103/PhysRevB.103.245418

I. INTRODUCTION

Superconducting states are difficult to reach as they require very strict laboratory parameters [1]. High-T_c superconductors use cuprates which are well-ordered structures of atoms combined in three-dimensional arrangements [2–7]. For these materials, the mechanism that counteracts the Colombian repulsion force between electrons is not exactly known, and for this reason, these unconventional states are referred to as strongly correlated [8,9]. Recently, it has been discovered that twisted bilayer graphene exhibits superconducting states at certain rotation angles [10,11] where the electron interactions are maximized [12]. This rotated graphene bilayer model generates a moiré pattern as a function of the rotation angle, defining a moiré Brillouin zone (mBZ) in reciprocal space. These special angles are called "magic" and were predicted as a possible consequence of flat bands observed in previous theoretical work [13]. In the work of Cao *et al.* [10], a Mott insulating state appears in the middle of these superconducting phases. The study of the electronic properties of rotated graphene over graphene started before the discovery of superconductivity at magic angles. In the work of J. Santos [14] and A. MacDonald [13], a continuous Hamiltonian model was presented; however, due to the presence of an interlayer amplitude AA coupling (see Fig. 1), this model did not present chiral symmetry. In a recent work by G. Tarnopolsky *et al.* [15], a chiral continuum model was studied, and only the AB and BA inter-layer couplings are different from zero. Perhaps, so far, it is the simplest model that best captures the nature of magic angles; at these angles the dispersion energy becomes flat and has a recurrence behavior. At these magic angles, the Fermi velocity also goes to zero. Due to its chiral symmetry, the Hamiltonian of this model also produces an intravalley inversion symmetry [16], so the energy dispersion is inversion symmetric at all twist angles. Also, we can distinguish between different magic angles when zero modes occurs, and thus the inter-valley inversion classifies the topology of the twist angle. The zero-mode flat-band solutions have some resemblance to the ground state of a quantum Hall effect wave function on a torus [15,17], and, therefore, the solution is of the harmonic oscillator type, where Landau levels arise [17–19]. The mechanism that causes the appearance of these magic angles is still not known, however, many investigations suggest that it is a topological aspect of the band structure [20–26]. The aim of this work its to clarify the physical behavior of this model and to develop an effective 2×2 effective Hamiltonian matrix by taking into account the particle-hole symmetry. This results in a folding of the spectrum around zero energy. Then we discuss the physical picture that arises from this renormalization by showing that at magic angles, the intralayer electron wave-function frustration is exactly zero. Also, our effective Hamiltonian clearly shows the presence of three main contributions: kinetic and confinement energies and a non-Abelian gauge potential. The layout of this paper is the following: we start with the model and renormalization in Sec. II, the corresponding physical picture is analyzed in Sec. III and the relationship with a rigidity phonon problem is discussed in Sec. IV. In Sec. V, we discuss how to write the effective Hamiltonian using Pauli matrices and triangular coordinates. Finally, the conclusions are given.

II. TWISTED BILAYER GRAPHENE EFFECTIVE MODEL

Tarnopolsky *et al.* derived a chiral Hamiltonian for electron-holes in twisted bilayer graphene. It captures the

*naumis@fisica.unam.mx

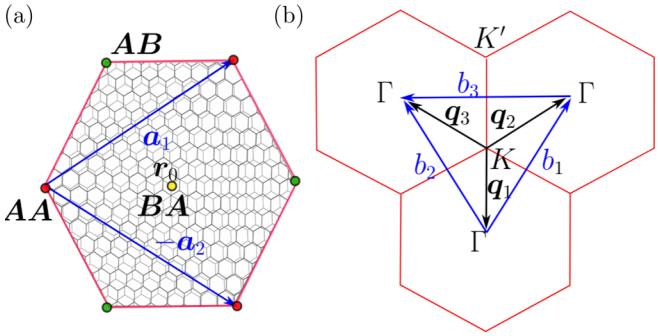

FIG. 1. (a) Real space moiré unit cell, $\boldsymbol{a_{1,2}}$ are two moiré lattice vectors. Point $\boldsymbol{r}_0 = (\boldsymbol{a}_1 - \boldsymbol{a}_2)/3$ is the BA stacking point where all components of the wave function vanish at magic α. (b) mBZ in reciprocal space, $\boldsymbol{b_{1,2}}$ are the base vectors.

"true magic" of the magic angle physics [15],

$$\mathcal{H} = \begin{pmatrix} 0 & D^*(-r) \\ D(r) & 0 \end{pmatrix}, \tag{1}$$

where the zero-mode operator is

$$D(r) = \begin{pmatrix} -i\bar{\partial} & \alpha U(r) \\ \alpha U(-r) & -i\bar{\partial} \end{pmatrix} \tag{2}$$

and

$$D^*(-r) = \begin{pmatrix} -i\partial & \alpha U^*(-r) \\ \alpha U^*(r) & -i\partial \end{pmatrix} \tag{3}$$

with $\bar{\partial} = \partial_x + i\partial_y$, $\partial = \partial_x - i\partial_y$. The potential is

$$U(\boldsymbol{r}) = e^{-i\boldsymbol{q}_1\cdot\boldsymbol{r}} + e^{i\phi}e^{-i\boldsymbol{q}_2\cdot\boldsymbol{r}} + e^{-i\phi}e^{-i\boldsymbol{q}_3\cdot\boldsymbol{r}}. \tag{4}$$

For this Hamiltonian, the parameters are $\phi = \frac{2\pi}{3}$ and $\boldsymbol{q}_1 = k_\theta(0,-1)$, $\boldsymbol{q}_2 = k_\theta(\frac{\sqrt{3}}{2}, \frac{1}{2})$ and $\boldsymbol{q}_3 = k_\theta(-\frac{\sqrt{3}}{2}, \frac{1}{2})$, the moiré modulation vector is $k_\theta = 2k_D \sin\frac{\theta}{2}$ with $k_D = \frac{4\pi}{3a_0}$ is the magnitude of the Dirac wave vector and a_0 is the lattice constant of monolayer graphene, see Fig. 1. The physics of this model is captured by the parameter α, defined as $\alpha = \frac{w_1}{v_0 k_\theta}$. Here w_1 is the interlayer coupling of stacking AB and BA, take the value $w_1 = 110$ meV and v_0 is the Fermi velocity, with value $v_0 = \frac{19.81eV}{2k_D}$. At magic angles $\alpha = 0.586,\ 2.221,\ 3.751,\ 5.276,\ 6.795,\ 8.313,\ 9.829,\ 11.345, \ldots$, flat bands appear. Magic α's follow a remarkable 3/2 quantization rule [15] for $\alpha > 0.586$.

This Hamiltonian is difficult to tackle and in fact most of the studies have been restricted to the zero-mode operator solutions at energy zero [16,17]. Here, instead of solving the Schrödinger equation with $\mathcal{H}$ we first propose to reduce the dimensionality of the problem. Starting with the Schrödinger equation $\mathcal{H}\Phi = E\Phi$, where $\Phi(r) = (\psi_1(r), \psi_2(r), \chi_1(r), \chi_2(r))^T$ are the four components of the twisted graphene bilayer, and the index 1,2 represent each graphene layer, we consider the squared Hamiltonian $\mathcal{H}^2$,

$$\mathcal{H}^2 = \begin{pmatrix} D^*(-r)D(r) & 0 \\ 0 & D(r)D^*(-r) \end{pmatrix}. \tag{5}$$

This transforms the off-diagonal blocks into zeros. We can understand such transformation as a removal of the particle-hole symmetry that is an antiunitary anti-symmetry. Therefore we obtain a decoupled equation $\mathcal{H}^2\Phi(r) = E^2\Phi(r)$, where the eigenvalues are the squares of the original energies. States at $E = 0$ are thus ground states of $\mathcal{H}^2\Phi(r)$. For arbitrary α, there are always two zero-mode solutions in the K and K' points [15], the signature of a magic angle in $\mathcal{H}^2$ is that the Fermi velocity at $\boldsymbol{k} = K, K'$ points of the Moiré Brillouin zone (mBZ) approaches zero and a massive degenerate ground state. We now define a 2×2 effective Hamiltonian $H^2 = D^*(-r)D(r)$. As detailed in Appendix A, the resulting effective Hamiltonian is

$$H^2 = \begin{pmatrix} -\nabla^2 + \alpha^2|U(-\boldsymbol{r})|^2 & \alpha A^\dagger(\boldsymbol{r}) \\ \alpha A(\boldsymbol{r}) & -\nabla^2 + \alpha^2|U(\boldsymbol{r})|^2 \end{pmatrix}. \tag{6}$$

The norm of the potential is

$$\begin{aligned} |U(\boldsymbol{r})|^2 =& 3 + 2\cos(\boldsymbol{b}_1\cdot\boldsymbol{r} - \phi) + 2\cos(\boldsymbol{b}_2\cdot\boldsymbol{r} + \phi) \\ &+ 2\cos(\boldsymbol{b}_3\cdot\boldsymbol{r} + 2\phi), \end{aligned} \tag{7}$$

where $\boldsymbol{b}_{1,2} = \boldsymbol{q}_{2,3} - \boldsymbol{q}_1$ are the mBrillouin zone moiré vectors and $\boldsymbol{b}_3 = \boldsymbol{q}_3 - \boldsymbol{q}_2$ (see Fig. 1). Notice the similarity with a triangular lattice energy dispersion Eq. (C12) but at the scale of the moiré pattern. The off-diagonal terms are

$$A(\boldsymbol{r}) = -i\sum_{\mu=1}^{3} e^{i\boldsymbol{q}_\mu\cdot\boldsymbol{r}}\left(2\hat{\boldsymbol{q}}_\mu^\perp\cdot\nabla - k_\theta\right) \tag{8}$$

and

$$A^\dagger(\boldsymbol{r}) = -i\sum_{\mu=1}^{3} e^{-i\boldsymbol{q}_\mu\cdot\boldsymbol{r}}\left(2\hat{\boldsymbol{q}}_\mu^\perp\cdot\nabla + k_\theta\right), \tag{9}$$

where $\nabla^\dagger = -\nabla$ with $\nabla = (\partial_x, \partial_y)$ and $\mu = 1, 2, 3$. This is an essential point as eigenvalues must be reals [notice that $-A^\dagger(-\boldsymbol{r}) = A(\boldsymbol{r})$]. Also, $\hat{\boldsymbol{q}}_\mu^\perp$ is a set of unitary vectors perpendicular to the set $\boldsymbol{q}_\mu$ (see Appendix A). The term $\hat{\boldsymbol{q}}_\mu^\perp\cdot\nabla$ is the directional gradient along the triangle defined by the moiré vectors and has an interpretation in terms of frustration (see next section) and is a kind of non-Abelian gauge field [27,28]. We see in H^2 three terms that define the physics of the problem: the kinetic energy (corresponding to the Laplacian), a confinement due to the potential and the non-Abelian gauge term that couples layers. Any eigenfunction of the original Hamiltonian is an eigenfunction of $\mathcal{H}^2$, therefore, the spinor $\Psi(\boldsymbol{r}) = (\psi_1(\boldsymbol{r}), \psi_2(\boldsymbol{r}))$ is a solution of H^2. In a similar way, we can proceed to use $D(r)D^*(-r)$ with solutions $(\chi_1(\boldsymbol{r}), \chi_2(\boldsymbol{r}))$. These solutions are easily obtained from $(\psi_1(\boldsymbol{r}), \psi_2(\boldsymbol{r}))$ using symmetry operations, and thus here we only study H^2. $\mathcal{H}^2$ eigenfunctions are made from a superposition of pseudospin polarized states of $\mathcal{H}$.

III. PHYSICAL INTERPRETATION OF THE EFFECTIVE MODEL AND FLAT BANDS

The renormalization into a 2×2 matrix not only simplifies the mathematics but has a profound physical meaning. What we achieved is the decoupling of the A and B bipartite lattices for each graphene layer. As we detail in Appendix C, for graphene such squared Hamiltonian is equivalent to renormalize the honeycomb lattice into a triangular lattice with renormalized interactions and a self-energy [29,30]. As sketched in Fig. 2 for monolayer graphene, the transformation

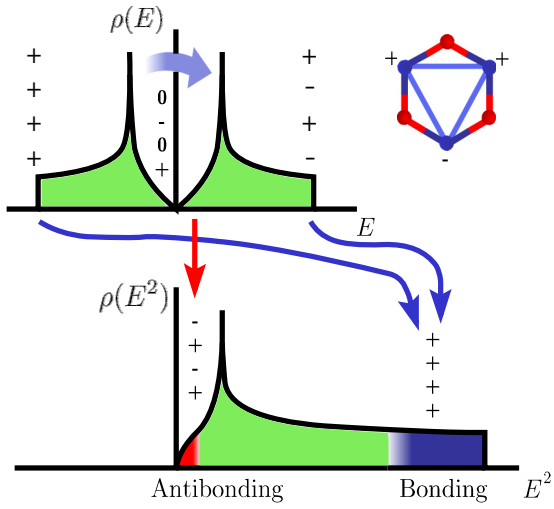

FIG. 2. For each noninteracting monolayer graphene case, we present the density of states $\rho(E)$ and of $\rho(E^2)$ corresponding to the squared Hamiltonian, equivalent to a folding of the spectrum. The signs are a sketch of the relative signs and amplitudes on bipartite sublattices A and B (shown in red and blue). Arrows indicate how the states are mapped under such transformation. Zero modes and close-by states are in the antibonding limit on a triangular lattice (indicated by the triangle inside the hexagon). The frustration is seen here in the bond that joins the + and + sites in the triangle (in reality, the minimal phase difference is ϕ). For the twisted bilayer with interlayer interaction, $\mathcal{H}^2$ produces a similar DOS folding and relative signs for the superlattice.

of E to E^2 produces a fold in the spectrum such that bonding states with the lowest energy are mapped into higher energies. In other words, the transformation deletes the alternating sign of one of the bipartite sublattices as explained in Fig. 2. Here our Eq. (6) shows that we have a similar situation as we detail below.

As zero modes are ground states of H^2, we end up having a clear picture of nearby states around zero-energy modes, they correspond to the antibonding limit in two coupled triangular lattices. However, as detailed in Appendix C, anti-bonding states in non-bipartite lattices are frustrated as they cannot achieve a phase difference of π between sites as odd-rings are present [31,32]. For disordered systems, states are localized in regions of lower frustration [33] and a kind of Lifshitz tail appears [32]. Moreover, frustration is always associated with massive degeneration [31,32,34]; it leads to Van Hove singularities or if possible, in a condensation of confined states. These confined states appear in chiral models of the Penrose lattice [35–37], where they form beautiful fractal patterns [36], in random binary alloys [38,39] and in graphene with defects [29,40]. Strictly confined states are degenerate. However, there is a basis in which the amplitude in one of the bipartite sublattices is zero while in the other, the sum of all neighbors amplitudes is always zero for any site [36,38].

To understand how zero modes are related with confined states and frustration as in Fig. 2 for twisted graphene bilayers, let us made the following remarks. From the Hamiltonian (1), we confirm that for $E = 0$ there are always solutions of the form $\Phi^A_{\boldsymbol{k}}(\boldsymbol{r}) = (\psi^A_{\boldsymbol{k},1}(\boldsymbol{r}), \psi^A_{\boldsymbol{k},2}(\boldsymbol{r}), 0, 0)$ and $\Phi^B_{\boldsymbol{k}}(\boldsymbol{r}) = (0, 0, \chi^B_{\boldsymbol{k},1}(\boldsymbol{r}), \chi^B_{\boldsymbol{k},2}(\boldsymbol{r}))$, where the labels A and B are used to denote zero amplitude in the opposite bipartite sublattice. We remark that linear combinations,

$$\Phi_{\boldsymbol{k}}(\boldsymbol{r}) = \frac{1}{\sqrt{2}}\left(\Phi^A_{\boldsymbol{k}}(\boldsymbol{r}) + e^{i\gamma}\Phi^B_{\boldsymbol{k}}(\boldsymbol{r})\right) \tag{10}$$

with γ a phase, result in a different basis, which does not show zeros in one sublattice, as for example with the symmetrized/antisymmetrized cases $\gamma = 0, \pi$. As the potential does not brake the C_3 symmetry, the states $\boldsymbol{k} = \boldsymbol{K}, \boldsymbol{K}'$ are always a $E = 0$ solution for any α. As a conclusion, for α not a magical angle there are four linearly independent wave functions, as confirmed from a Wronskian analysis [17] and therefore, at any angle there are "confined states" in the sense of Fig. 2. At magic angles, the Wronskian of the solutions is zero and there are $E = 0$ solutions at any $\boldsymbol{k}$, resulting in the flat band. Still, $\Phi^A_{\boldsymbol{k}}(\boldsymbol{r})$ and $\Phi^B_{\boldsymbol{k}}(\boldsymbol{r})$ are solutions meaning that now all states are "confined." Any linear combination using different sets of $\boldsymbol{k}$ is a solution. As explained below, this is similar to the Van-Hove singularity in monolayer graphene, where dimers are disconnected from the lattice and thus can be thought as a kind of highly degenerated confined state.

As we detail in Appendix C, the antibonding or bonding nature and therefore frustration is obtained from all bonds energy contribution, the latter one obtained from the product of the wave function in a site with the conjugated wave function of a neighboring site [39]. For the present system, this requires to take into account three factors: (1) the system has two layers, (2) we are dealing with a low-energy continuous version of the original tight-binding model, and (3) the system has a superlattice. Concerning point 1, we look at the intralayer frustration to see how the interlayer interaction tunes such contribution. Points 2 and 3 are more delicate as we need to understand that k is a moment that departs from K and K'. In a two-layer bipartite continuous lattice, for a given state $\boldsymbol{k}$ such procedure is equivalent to consider bonds joining A and B sublattices sites. Although this can be made using any basis, it is easier to use in a symmetrized one $\gamma = 0$.

To see how the interlayer contributions tunes the frustration between layers, the local intralayer frustration is obtained from the function (see Appendix C),

$$g_{\boldsymbol{k}}(\boldsymbol{r}) = \psi_{\boldsymbol{k},1}(\boldsymbol{r})\chi^*_{\boldsymbol{k},1}(\boldsymbol{r}) + \psi_{\boldsymbol{k},2}(\boldsymbol{r})\chi^*_{\boldsymbol{k},2}(\boldsymbol{r}), \tag{11}$$

which contains the relative phases between each pair of neighbors, in this case applied to each graphene layer. As we are interested in states near $E = 0$, we set $\boldsymbol{k} = \boldsymbol{K}$ in Eq. (11). Using the symmetry of the problem, we can show that $\chi^*_{\boldsymbol{K}}(\boldsymbol{r}) = \psi_{\boldsymbol{K}}(-\boldsymbol{r})$ and

$$g_{\boldsymbol{K}}(\boldsymbol{r}) = \psi_{\boldsymbol{K},1}(\boldsymbol{r})\psi_{\boldsymbol{K},1}(-\boldsymbol{r}) + \psi_{\boldsymbol{K},2}(\boldsymbol{r})\psi_{\boldsymbol{K},2}(-\boldsymbol{r}) \sim v_F(\alpha) \tag{12}$$

where this last step is obtained from the fact that $g_{\boldsymbol{K}}$ turns out to be an invariant (see Appendix B), which can be identified with the Fermi velocity at a given angle [15], here denoted by $v_F(\alpha)$. At magic angles $v_F(\alpha) = 0$ and therefore also $g_{\boldsymbol{K}} = 0$, i.e., frustration is zero, making a flat band by pushing all states towards $E = 0$.

As $g_{\boldsymbol{K}}(\boldsymbol{r}) = v_F(\alpha)$, we have that $\nabla g_{\boldsymbol{K}}(\boldsymbol{r}) = 0$. Thus, from Eq. (14), we conclude that as expected the ground state is

always the minimally frustrated state for all α and that the total frustration is,

$$F(\boldsymbol{k}) \approx \int_S d^2\boldsymbol{r}|g_{\boldsymbol{k}}(\boldsymbol{r})|^2 = v_F^2(\alpha) \tag{13}$$

At magic angles, $F(\boldsymbol{k}) = 0$. Finally, notice some similarity of the gradient term in Eq. (14) and the term $A(\boldsymbol{r})$ in the squared Hamiltonian as we can write by using the symmetry that

$$F(\boldsymbol{k}) \approx \int_S d^2\boldsymbol{r} g^*_{\boldsymbol{k}}(\boldsymbol{r})\left(g_{\boldsymbol{k}}(\boldsymbol{r}) + \sum_{s=1}^{3} \bar{\boldsymbol{a}}_s \cdot \nabla[g_{\boldsymbol{k}}(\boldsymbol{r}) + g_{\boldsymbol{k}}(-\boldsymbol{r})]\right), \tag{14}$$

where $\bar{\boldsymbol{a}}_s$ points to the layer underlying trigonal lattice vertices. In $A(\boldsymbol{r})$, $e^{i\boldsymbol{q}_\mu\cdot\boldsymbol{r}}$ is the phase difference between neighbors due only to geometrical reasons multiplied by the gradient of the local phase difference $\hat{q}^\perp_\mu \cdot \nabla$. In $A(\boldsymbol{r})$, the k_θ term will give the averaged geometrical phase difference over all space once its expectation value is calculated.

The fine tuning required to have zero-frustration leads to a special condition for the wave function Fourier components. The explicit form of the wave function is

$$\psi_{\boldsymbol{k}}(\boldsymbol{r}) = \sum_{m,n}\begin{pmatrix} a_{mn} \\ b_{mn}e^{i\boldsymbol{q}_1\cdot\boldsymbol{r}}\end{pmatrix} e^{i(\boldsymbol{K}_{mn}+\boldsymbol{k})\cdot\boldsymbol{r}}, \tag{15}$$

where $\boldsymbol{K}_{mn} = m\boldsymbol{b}_1 + n\boldsymbol{b}_2$. $a_{m,n}$ and $b_{m,n}$ are the Fourier coefficients. At the BA stacking point $\boldsymbol{r}_0 = (\boldsymbol{a}_1 - \boldsymbol{a}_2)/3$, and for any α and due to symmetry reasons $\psi_{\boldsymbol{K},2}(\boldsymbol{r}_0)\psi_{\boldsymbol{K},2}(-\boldsymbol{r}_0) = 0$, while for magic α we have that [15] $\psi_{\boldsymbol{K},1}(\boldsymbol{r}_0) = 0$.

Consider the particular case $\boldsymbol{r} = \boldsymbol{r}_0$ and $\boldsymbol{k} = \boldsymbol{K} = 0$ as the $\boldsymbol{K}$ point is at the origin. We have

$$\begin{aligned}\boldsymbol{K}_{mn}\cdot\boldsymbol{r}_0 &= \boldsymbol{K}_{mn}\cdot\left(\frac{\boldsymbol{a}_1 - \boldsymbol{a}_2}{3}\right) \\ &= \frac{1}{3}(m\boldsymbol{b}_1 + n\boldsymbol{b}_2)\cdot(\boldsymbol{a}_1 - \boldsymbol{a}_2),\end{aligned} \tag{16}$$

where we used that $\boldsymbol{b}_i \cdot \boldsymbol{a}_j = 2\pi\delta_{ij}$. Then we obtain

$$\begin{aligned}\psi_{\boldsymbol{K},1}(\boldsymbol{r}_0) &= \sum_{m,n} a_{mn}e^{i\boldsymbol{K}_{mn}\cdot\boldsymbol{r}_0} \\ &= \sum_{m,n} a_{mn}e^{i(m-n)\phi}\end{aligned} \tag{17}$$

while

$$\begin{aligned}\psi_{\boldsymbol{K},2}(\boldsymbol{r_0}) &= \sum_{m,n} b_{mn}e^{-i\boldsymbol{K}_{mn}\cdot\boldsymbol{r}_0} \\ &= \sum_{m,n} b_{mn}e^{-i(m-n)\phi}\end{aligned} \tag{18}$$

but with the extra conditions

$$\begin{aligned}\psi_{\boldsymbol{K},2}(\boldsymbol{r_0} \pm \boldsymbol{a_1}) &= e^{\pm i\phi}\sum_{m,n} b_{mn}e^{-i\boldsymbol{K}_{mn}\cdot\boldsymbol{r}_0} \\ &= e^{\pm i\phi}\psi_{\boldsymbol{K},2}(\boldsymbol{r_0}).\end{aligned} \tag{19}$$

At magic angles $\psi_{\boldsymbol{k},1}(\boldsymbol{r}_0) = 0$ from where,

$$\sum_{m,n} a_{mn}(e^{i(m-n)\phi} + e^{-i(m-n)\phi}) = 0 \tag{20}$$

with $\phi = 2\pi/3$. By a simple analysis of the phases, we obtain the condition at magic angles,

$$\sum_{m,s}\left(a_{m,3s} + a_{m,3s+1}e^{i\phi} + a_{m,3s-1}e^{-i\phi}\right) = 0. \tag{21}$$

The same equation holds for b_{mn}. The previous equation shows a precise tuning of components and hints how the electron density tends to develop sharp local maxima as $\alpha \to \infty$, in agreement with the quantum dot picture of the problem [41].

IV. FLAT BANDS IN TWISTED GRAPHENE BILAYERS AS FLOPPY MODES IN A RIGIDITY THEORY OF PHONONS

Quite surprisingly, our renormalization is akin to a phonon problem, and the flat-band can be interpreted as a massive zero frequency vibrational band, since E^2 is analogous to a frequency. These floppy modes are well known in the Phillips rigidity theory of glasses [42] and are reminiscent of the protected electronic boundary modes that occur in the quantum Hall effect and in topological insulators [43].

To understand this, let us start in the limiting case where $\alpha \to 0$. The TBG Hamiltonian reduces to

$$\mathcal{H}(r) = \begin{pmatrix} 0 & D^*(-r) \\ D(r) & 0\end{pmatrix}, \tag{22}$$

where

$$D(r) \approx \begin{pmatrix} -i\bar{\partial} & 0 \\ 0 & -i\bar{\partial}\end{pmatrix}, \quad \bar{\partial} = \partial_x + i\partial_y. \tag{23}$$

Therefore, if we take $\boldsymbol{k} = (k_x + ik_y)\sigma_0$, we have that the Hamiltonian in momentum space is given by

$$\mathcal{H}(k) = \begin{pmatrix} 0 & \boldsymbol{k}^* \\ \boldsymbol{k} & 0\end{pmatrix}. \tag{24}$$

Using the relation $\chi(r) = \Psi^*_K(-r)$, as is done in Ref. [15], one gets the following expression for the Fermi velocity:

$$v_F(\alpha) = \frac{|\langle\Psi^*_K(-r)||\Psi_K(r)\rangle|}{|\langle\Psi^*_K(r)||\Psi_K(r)\rangle|}. \tag{25}$$

Expression (25) is independent of k since $|\partial_k\mathcal{E}(k)| = v_F(\alpha)$ is constant, here $\mathcal{E} = \hbar w(k)$. As a result we have that

$$v_F(\alpha)|k| = \mathcal{E}(k). \tag{26}$$

If we take $\hbar$=1, Eq. (26) implies

$$w(k) = v_F(\alpha)|k|. \tag{27}$$

We can achieve a better understanding of $v_F(\alpha)$ using Eq. (27) and the connection established in Ref. [43] with floppy modes. In Ref. [43], the authors develop a dynamic matrix $\mathcal{D} = QQ^T$ with eigenvalues w_n^2. In our paper, a direct relation is drawn among $\mathcal{H}^2 = D^*(-r)D(r)$ and $\mathcal{D}$. Now w_n^2 are eigenvalues of $\mathcal{H}^2$. Consequently, $v_F(\alpha)$ is analogous to the speed of sound. Therefore, at magic α, $v_F(\alpha)$ is zero and a massive degeneracy is found. This is exactly the case of the floppy mode peak which occurs at zero frequency [44–47]. These modes have the property of being deformations without elastic energy cost, available due to the lack of mechanical constraints when compared with the number degrees of freedom [42]. It

seems that here α somehow controls the effective number of constrains.

V. EFFECTIVE FIELDS AND HAMILTONIAN IN TRIANGULAR COORDINATES

It is useful to write the renormalized twisted graphene bilayer Hamiltonian in terms of the Pauli matrix vector $\hat{\boldsymbol{\sigma}}$ as follows:

$$H^2 = h_0(\boldsymbol{r})\sigma_0 + \boldsymbol{h}(\boldsymbol{r})\cdot\hat{\boldsymbol{\sigma}}, \tag{28}$$

where the vector $\boldsymbol{h}(\boldsymbol{r})$ is

$$\boldsymbol{h}(\boldsymbol{r}) = (\alpha h_x(\boldsymbol{r}), \alpha h_y(\boldsymbol{r}), \alpha^2 h_z(\boldsymbol{r})) \tag{29}$$

with

$$\begin{aligned} h_x(\boldsymbol{r}) &= -\sum_\mu [k_\theta \sin(\boldsymbol{q}_\mu\cdot\boldsymbol{r}) + 2i\cos(\boldsymbol{q}_\mu\cdot\boldsymbol{r})\hat{\boldsymbol{q}}_\mu^\perp\cdot\nabla], \\ h_y(\boldsymbol{r}) &= \sum_\mu [k_\theta \cos(\boldsymbol{q}_\mu\cdot\boldsymbol{r}) - 2i\sin(\boldsymbol{q}_\mu\cdot\boldsymbol{r})\hat{\boldsymbol{q}}_\mu^\perp\cdot\nabla], \\ h_z(\boldsymbol{r}) &= \frac{|U(-\boldsymbol{r})|^2 - |U(\boldsymbol{r})|^2}{2}. \end{aligned} \tag{30}$$

The operator in front of the identity σ_0 is

$$h_0(\boldsymbol{r}) = -\nabla^2 + \alpha^2\bar{V}(\boldsymbol{r}), \tag{31}$$

$$\bar{V}(\boldsymbol{r}) = \frac{|U(\boldsymbol{r})|^2 + |U(-r)|^2}{2}. \tag{32}$$

We observe that $h_0(\boldsymbol{r})$ corresponds to a Hamiltonian with an average potential. The Hamiltonian structure is akin to the one found in Ref. [28]. Observe that the term $\boldsymbol{h}(\boldsymbol{r})$ contains all the topological properties of the operator. Moreover, as the three Pauli matrices are present, there is no rotation that produces a real and symmetric Hamiltonian, therefore time-reversal invariance is broken explicitly. Let us further simplify this Hamiltonian. Define $\psi_\pm(\boldsymbol{r}) = \psi_1(\boldsymbol{r}) \pm \psi_2(\boldsymbol{r})$. The Schrödinger equation is transformed into $H_{\text{eff}}(\psi_+(\boldsymbol{r}), \psi_-(\boldsymbol{r}))^T = E^2(\psi_+(\boldsymbol{r}), \psi_-(\boldsymbol{r}))^T$. The stated effective Hamiltonian is

$$H_{\text{eff}} = \begin{pmatrix} -\nabla^2 + V_{\text{eff}}(\boldsymbol{r}) & A^\dagger_{\text{eff}}(\boldsymbol{r}) \\ A_{\text{eff}}(\boldsymbol{r}) & -\nabla^2 + V_{\text{eff}}(\boldsymbol{r}) \end{pmatrix}. \tag{33}$$

Here we defined the effective potentials as

$$V_{\text{eff}}(\boldsymbol{r}) = \alpha^2\bar{V}(\boldsymbol{r}) + \alpha h_x(\boldsymbol{r}) \tag{34}$$

and

$$A_{\text{eff}}(\boldsymbol{r}) = \alpha^2 h_z(\boldsymbol{r}) + i\alpha h_y(\boldsymbol{r}). \tag{35}$$

Next we show how this Hamiltonian can be further simplified by using triangular coordinates and thus map the problem into a friendly rectangular domain. Due to the symmetry, we introduce the triangular coordinates u_j with $u_1 = \boldsymbol{b}_1\cdot\boldsymbol{r}$, $u_2 = -\boldsymbol{b}_2\cdot\boldsymbol{r}$, $u_3 = \boldsymbol{b}_3\cdot\boldsymbol{r}$. This transformation has the important property that $\sum_j u_j = 0$ and gives the distance to the edges of a triangle as seen in Fig. 3. Putting this transformation in the potential we get $\bar{V}(\boldsymbol{r}) = 3 - \sum_j \cos u_j$ and $h_z(\boldsymbol{r}) = -\sqrt{3}\sum_j \sin u_j$. A second change of variable is useful to reduce the Hamiltonian by taking into account mirror symmetries. We use, $\zeta = u_1$ and $\eta = u_2 - u_3$, where $0 \leqslant \eta \leqslant 4\pi$ and $0 \leqslant \zeta \leqslant 4\pi$. ζ and η are coordinates that indicate the departure from or along the median of the triangle. The inverse transformation is $u_2 = (\eta - \zeta)/2$ and $u_3 = -(\eta + \zeta)/2$. The average and Zeeman like terms are

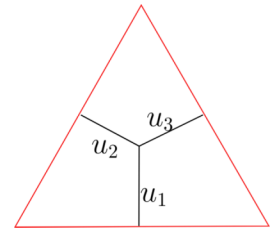

FIG. 3. Triangular coordinates.

$$\bar{V}(\boldsymbol{r}) = 3 - \cos\zeta - 2\cos\frac{\zeta}{2}\cos\frac{\eta}{2}, \tag{36}$$

$$h_z(\boldsymbol{r}) = -\sqrt{3}\left(\sin\zeta - 2\sin\frac{\zeta}{2}\cos\frac{\eta}{2}\right), \tag{37}$$

and the Laplacian operator is

$$\nabla^2 = 3k_\theta^2(\partial_\zeta^2 + 3\partial_\eta^2). \tag{38}$$

To reduce the other terms, we introduce an intermediate change of variable $\boldsymbol{q}_\mu\cdot\boldsymbol{r} = s_\mu$,

$$\begin{aligned} h_x(\boldsymbol{r}) = &-\sum_\mu k_\theta \sin s_\mu - 2i\left[\cos s_1 - \frac{\cos s_2 + \cos s_3}{2}\right]\partial_x \\ &- i\sqrt{3}[\cos s_2 - \cos s_3]\partial_y \end{aligned} \tag{39}$$

while

$$\begin{aligned} h_y(\boldsymbol{r}) = &\sum_\mu k_\theta \cos s_\mu - 2i\left[\sin s_1 - \frac{\sin s_2 + \sin s_3}{2}\right]\partial_x \\ &- i\sqrt{3}[\sin s_2 - \sin s_3]\partial_y. \end{aligned} \tag{40}$$

Then, we use the transformation into the ζ and η coordinates by first observing that $u_1 = s_2 - s_1$, $u_2 = s_1 - s_3$, and $u_3 = s_3 - s_2$, and finally,

$$s_1 = \frac{\eta - 3\zeta}{6}, \quad s_2 = \frac{\eta + 3\zeta}{6}, \quad s_3 = -\frac{\eta}{3}, \tag{41}$$

where $s_1 = -(s_2 + s_3)$ and

$$\partial_x = \frac{\sqrt{3}}{2}k_\theta(\partial_\zeta - 3\partial_\eta), \quad \partial_y = \frac{3}{2}k_\theta(\partial_\zeta + \partial_\eta). \tag{42}$$

In ζ and η coordinates, we have

$$\begin{aligned} \frac{h_x(r)}{k_\theta} = &\left(\sin\frac{\eta}{3} - 2\cos\frac{\zeta}{2}\sin\frac{\eta}{6}\right) \\ &- i2\sqrt{3}\left(\cos\frac{\zeta}{2}\cos\frac{\eta}{6} - \cos\frac{\eta}{3}\right)\partial_\zeta \\ &+ i6\sqrt{3}\sin\frac{\zeta}{2}\sin\frac{\eta}{6}\partial_\eta \end{aligned} \tag{43}$$

and

$$\begin{aligned} \frac{h_y(r)}{k_\theta} = &\left(\cos\frac{\eta}{3} + 2\cos\frac{\zeta}{2}\cos\frac{\eta}{6}\right) \\ &- i2\sqrt{3}\left(\cos\frac{\zeta}{2}\sin\frac{\eta}{6} + \sin\frac{\eta}{3}\right)\partial_\zeta \\ &- i6\sqrt{3}\sin\frac{\zeta}{2}\cos\frac{\eta}{6}\partial_\eta. \end{aligned} \tag{44}$$

Therefore we have all expressions for our effective Hamiltonian in terms of the triangular coordinates, i.e., $H_{\rm eff} = H_{\rm eff}(\zeta, \eta)$, and more importantly, in a rectangular domain amenable to numerical and analytical calculations. We end up this section by observing how the results indicate that we can scale the operator H^2 by defining $\alpha' = \alpha/k_\theta$ and $\epsilon = E/k_\theta$, in such a way that k_θ is no longer in the Hamiltonian, while we make the replacement $\alpha \to \alpha'$ and $E \to \epsilon$. In fact, such effective parameters can be found right away from the start by defining a scaled set of coordinates,

$$\boldsymbol{r}' = k_\theta \boldsymbol{r}, \quad \boldsymbol{q}'_\mu = \frac{\boldsymbol{q}_\mu}{k_\theta}. \tag{45}$$

This transformation maps the k_θ dependent basis vectors of the unitary cell into the k_θ independent basis vectors $\boldsymbol{a}'_{1,2} = 4\pi/3(\pm\sqrt{3}, 1/2)$. Although is possible to make this scaling of the full Hamiltonian right from the start, in our development, we decided to stick with the notation used by others in previous works and keep this argument as a cross-check point.

VI. CONCLUSIONS

We showed that the chiral Hamiltonian for twisted graphene bilayers can be written as a 2×2 matrix operator. The operator has three contributions, a kinetic term, a confining potential and a non-Abelian gauge field. The action of the proposed renormalization maps the zero-mode region into the ground state. Modes next to zero energy have an antibonding nature in a triangular lattice and at zero energy are similar to confined modes observed in many other bipartite systems [37–39]. Then we showed that at magic angles, the intralayer electron wave-function frustration is exactly zero. A surprising result is that our renormalization suggests that flat band are somehow analogous to floppy modes in rigidity phonon models.

ACKNOWLEDGMENTS

We thank UNAM-DGAPA Project No. IN102620 and CONACyT Project No. 1564464. We also thank Francisco Guinea and Pierre A. Pantaleón (Imdea Nanoscience), Jie Wang (Flatiron Institute), Patrick Ledwith (Harvard University), Saúl Herrera, Elías Andrade, and David Ruiz Tijerina (IF-UNAM) for useful comments on this project.

APPENDIX A: EXPLICIT CALCULATION OF H^2

We write the potential as

$$U(\boldsymbol{r}) = (1, e^{i\phi}, e^{-i\phi}) \cdot \left(e^{-is_1}, e^{-is_2}, e^{-is_3}\right). \tag{A1}$$

This suggest to define a tensorial form as $U(\boldsymbol{r}) = \boldsymbol{e} \cdot \boldsymbol{S}(\boldsymbol{r}) = e_\mu S_\mu$, where $\mu = 1, 2, 3$ and the Einstein sum rule is applied to repeated dummy indices. The components of the vectors $\boldsymbol{e}$ and $\boldsymbol{S}(\boldsymbol{r})$ are

$$e_\mu = e^{i(\mu-1)\phi} \tag{A2}$$

and

$$S_\mu(\boldsymbol{r}) = e^{-is_\mu}. \tag{A3}$$

Using the tensorial definition of the potential, we have

$$\begin{aligned} |U(\boldsymbol{r})|^2 &= U^*(\boldsymbol{r})U(\boldsymbol{r}) \\ &= \sum_{\mu,\nu} \left(e^{-i(\nu-1)\phi} e^{is_\nu}\right)\left(e^{i(\mu-1)\phi} e^{-is_\mu}\right) \\ &= \sum_{\mu,\nu} e^{i(\mu-\nu)\phi} e^{i(s_\nu - s_\mu)}. \end{aligned} \tag{A4}$$

Working with the upper block Hamiltonian $H^2 = D^*(-r)D(r)$, we have that the initial expression is

$$H^2 = \begin{pmatrix} -\nabla^2 + \alpha^2|U(-r)|^2 & -i\alpha(U^*(-r)\bar{\partial} + \partial U(r)) \\ -i\alpha(U^*(r)\bar{\partial} + \partial U(-r)) & -\nabla^2 + \alpha^2|U(r)|^2 \end{pmatrix}. \tag{A5}$$

Then, the eigenvalue equation is $H^2\Psi(r) = E^2\Psi(r)$, with the spinor $\Psi(r) = (\Psi_1(r), \quad \Psi_2(r))^T$. Here its convenient to define the operators:

$$\begin{aligned} B_1(r) &= -i[U^*(r)\bar{\partial} + \partial U(-r)], \\ B_2(r) &= -i[\partial U(r) + U^*(-r)\bar{\partial}]. \end{aligned} \tag{A6}$$

Focussing on the off-diagonal terms, we first multiply $B_1(r)$ with respect to the component spinor, so, we have

$$\begin{aligned} B_1(r)\psi_2(r) = -i[&U^*(r)\bar{\partial}\Psi_2(r) + \Psi_2(r)\partial U(-r) \\ &+ U(-r)\partial\Psi_2(r)]. \end{aligned} \tag{A7}$$

However, note that

$$\begin{aligned} \partial U(-r) &= \sum_\mu e^{i(\mu-1)\phi}\partial e^{is_\mu} = \sum_\mu e^{i(\mu-1)\phi}(\partial_x - i\partial_y)e^{is_\mu} \\ &= \sum_\mu e^{i(\mu-1)\phi}\left(iq^x_\mu - i\left(iq^y_\mu\right)\right)e^{is_\mu} \\ &= -k_\theta \sum_\mu e^{is_\mu}, \end{aligned} \tag{A8}$$

where we used that $q^x_\mu + iq^y_\mu = -ik_\theta e^{i(\mu-1)\phi}$, so, $q^x_\mu - iq^y_\mu = ik_\theta e^{-i(\mu-1)\phi}$. Substituting this result into $B_1(r)$, we get

$$\begin{aligned} B_1(r) &= -i[U^*(r)\bar{\partial} + \partial U(-r) + U(-r)\partial] \\ &= -i(U^*(r)\bar{\partial} - k_\theta \sum_\mu e^{is_\mu} + U(-r)\partial]. \end{aligned} \tag{A9}$$

Therefore

$$\begin{aligned} B_1(r) &= -i\sum_\mu e^{is_\mu}[e^{-i(\mu-1)\phi}\bar{\partial} - k_\theta + e^{i(\mu-1)\phi}\partial] \\ &= -i\sum_\mu e^{is_\mu}[-k_\theta + 2\hat{q}^\perp_\mu \cdot \nabla], \end{aligned} \tag{A10}$$

where we define, $\hat{q}^\perp_\mu = (\cos[(\mu-1)\phi], \sin[(\mu-1)\phi])$, this is a unitary vector perpendicular to $\boldsymbol{q}_\mu$ and $\nabla = (\partial_x, \partial_y)$ is the gradient. In a similar way, we calculate $B_2(r)$:

$$\begin{aligned} B_2(r)\Psi_1(r) = -i[&U(r)\partial\Psi_1(r) + \Psi_1(r)\partial U(r) \\ &+ U^*(-r)\bar{\partial}\Psi_1(r)] \end{aligned} \tag{A11}$$

and

$$\partial U(r) = \sum_{\mu} e^{i(\mu-1)\phi}\partial e^{-is_\mu} = \sum_{\mu} e^{i(\mu-1)\phi}(\partial_x - i\partial_y)e^{-is_\mu}$$
$$= \sum_{\mu} e^{i(\mu-1)\phi}(-iq_\mu^x - i(-iq_\mu^y))e^{-is_\mu}. \quad \text{(A12)}$$

Using this result in $B_2(r)$, we get

$$\begin{aligned} B_2(r) &= -i[U(r)\partial + \partial U(r) + U^*(-r)\bar{\partial}] \\ &= -i[U^*(-r)\bar{\partial} + k_\theta \sum_{\mu} e^{-is_\mu} + U(r)\partial] \\ &= -i\sum_{\mu} e^{-is_\mu}[k_\theta + e^{-i(\mu-1)\phi}\bar{\partial} + e^{i(\mu-1)\phi}\partial] \\ &= -i\sum_{\mu} e^{-is_\mu}[k_\theta + e^{-i(\mu-1)\phi}\bar{\partial} + e^{i(\mu-1)\phi}\partial]. \end{aligned} \quad \text{(A13)}$$

When comparing $B_1(r)$ and $B_2(r)$, we see that the relation $B_1^\dagger(r) = B_2(r)$ is satisfied. Therefore it is convenient to change, $B_1(r) = A(r)$ and $B_2(r) = A^\dagger(r)$, where $A(r)$ is a non-Abelian potential.

APPENDIX B: INVARIANT AND THE FERMI VELOCITY

Consider a zero-mode condition

$$D(\boldsymbol{r})\begin{pmatrix}\Psi_{\boldsymbol{k},1}(\boldsymbol{r})\\ \Psi_{\boldsymbol{k},2}(\boldsymbol{r})\end{pmatrix} = \begin{pmatrix}0\\0\end{pmatrix}, \quad \text{(B1)}$$

where $\Psi_{\boldsymbol{k},1}(\boldsymbol{r}) = e^{i\boldsymbol{k}\cdot\boldsymbol{r}}u_{\boldsymbol{k},1}(\boldsymbol{r})$ and $\Psi_{\boldsymbol{k},2}(\boldsymbol{r}) = e^{i\boldsymbol{k}\cdot\boldsymbol{r}}u_{\boldsymbol{k},2}(\boldsymbol{r})$. For $\boldsymbol{k} = \boldsymbol{K} = 0$, it follows that

$$D(\boldsymbol{r})\begin{pmatrix}\Psi_{\boldsymbol{k},1}(\boldsymbol{r})\\ \Psi_{\boldsymbol{k},2}(\boldsymbol{r})\end{pmatrix} = \begin{pmatrix}-i\bar{\partial} & \alpha U(\boldsymbol{r})\\ \alpha U(-\boldsymbol{r}) & -i\bar{\partial}\end{pmatrix}\begin{pmatrix}u_{\boldsymbol{k},1}(\boldsymbol{r})\\ u_{\boldsymbol{k},2}(\boldsymbol{r})\end{pmatrix} = \begin{pmatrix}0\\0\end{pmatrix}. \quad \text{(B2)}$$

Therefore we get

$$-i\bar{\partial}u_{\boldsymbol{K},1}(\boldsymbol{r}) + \alpha U(\boldsymbol{r})u_{\boldsymbol{K},2}(\boldsymbol{r}) = 0 \quad \text{(B3)}$$

and

$$\alpha U(-\boldsymbol{r})u_{\boldsymbol{K},1}(\boldsymbol{r}) - i\bar{\partial}u_{\boldsymbol{K},2}(\boldsymbol{r}) = 0. \quad \text{(B4)}$$

Multiply by $u_{\boldsymbol{K},1}(-\boldsymbol{r})$ in Eq. (B3) and $u_{\boldsymbol{K},2}(-\boldsymbol{r})$ in Eq. (B4). We have

$$\alpha U(-\boldsymbol{r})u_{\boldsymbol{K},1}(-\boldsymbol{r})u_{\boldsymbol{K},1}(\boldsymbol{r}) - iu_{\boldsymbol{K},1}(-\boldsymbol{r})\bar{\partial}u_{\boldsymbol{K},2}(\boldsymbol{r}) = 0 \quad \text{(B5)}$$

and

$$\alpha U(-\boldsymbol{r})u_{\boldsymbol{K},2}(-\boldsymbol{r})u_{\boldsymbol{K},1}(\boldsymbol{r}) - iu_{\boldsymbol{K},2}(-\boldsymbol{r})\bar{\partial}u_{\boldsymbol{K},2}(\boldsymbol{r}) = 0, \quad \text{(B6)}$$

respectively. Changing $\boldsymbol{r}' \to -\boldsymbol{r}$ in the last equation,

$$\alpha U(\boldsymbol{r}')u_{\boldsymbol{K},2}(\boldsymbol{r}')u_{\boldsymbol{K},1}(-\boldsymbol{r}') + iu_{\boldsymbol{K},2}(\boldsymbol{r}')\bar{\partial}u_{\boldsymbol{K},2}(-\boldsymbol{r}') = 0. \quad \text{(B7)}$$

Subtracting equation Eq. (B7) to Eq. (B5) and ignoring primes,

$$i(u_{\boldsymbol{K},2}(\boldsymbol{r})\bar{\partial}u_{\boldsymbol{K},2}(-\boldsymbol{r}) + u_{\boldsymbol{K},1}(-\boldsymbol{r})\bar{\partial}u_{\boldsymbol{K},1}(\boldsymbol{r})) = 0. \quad \text{(B8)}$$

On the other hand,

$$\begin{aligned} &\bar{\partial}(u_{\boldsymbol{K},1}(\boldsymbol{r})u_{\boldsymbol{K},1}(-\boldsymbol{r}) + u_{\boldsymbol{K},2}(\boldsymbol{r})u_{\boldsymbol{K},2}(-\boldsymbol{r})) \\ &= u_{\boldsymbol{K},2}(\boldsymbol{r})\bar{\partial}u_{\boldsymbol{K},2}(-\boldsymbol{r}) + u_{\boldsymbol{K},2}(-\boldsymbol{r})\bar{\partial}u_{\boldsymbol{K},2}(\boldsymbol{r}) \\ &\quad + u_{\boldsymbol{K},1}(-\boldsymbol{r})\bar{\partial}u_{\boldsymbol{K},1}(\boldsymbol{r}) + u_{\boldsymbol{K},1}(\boldsymbol{r})\bar{\partial}u_{\boldsymbol{K},1}(-\boldsymbol{r}), \end{aligned} \quad \text{(B9)}$$

but using Eq. (B8), we find the relation

$$\begin{aligned} &\bar{\partial}(u_{\boldsymbol{K},1}(\boldsymbol{r})u_{\boldsymbol{K},1}(-\boldsymbol{r}) + u_{\boldsymbol{K},2}(\boldsymbol{r})u_{\boldsymbol{K},2}(-\boldsymbol{r})) \\ &= u_{\boldsymbol{K},1}(\boldsymbol{r})\bar{\partial}u_{\boldsymbol{K},1}(-\boldsymbol{r}) + u_{\boldsymbol{K},2}(-\boldsymbol{r})\bar{\partial}u_{\boldsymbol{K},2}(\boldsymbol{r}) \end{aligned} \quad \text{(B10)}$$

changing $\boldsymbol{r} \to -\boldsymbol{r}'$ and by comparison to Eq. (B9) we can write last equation as

$$\bar{\partial}(u_{\boldsymbol{K},1}(\boldsymbol{r})u_{\boldsymbol{K},1}(-\boldsymbol{r}) + u_{\boldsymbol{K},2}(\boldsymbol{r})u_{\boldsymbol{K},2}(-\boldsymbol{r})) = 0. \quad \text{(B11)}$$

Therefore this equation gives a invariant and its follows that

$$v(\alpha) = u_{\boldsymbol{K},1}(\boldsymbol{r})u_{\boldsymbol{K},1}(-\boldsymbol{r}) + u_{\boldsymbol{K},2}(\boldsymbol{r})u_{\boldsymbol{K},2}(-\boldsymbol{r}), \quad \text{(B12)}$$

or using $\Psi_{\boldsymbol{K}} = u_{\boldsymbol{K}}$,

$$v(\alpha) = \Psi_{\boldsymbol{K},1}(\boldsymbol{r})\Psi_{\boldsymbol{K},1}(-\boldsymbol{r}) + \Psi_{\boldsymbol{K},2}(\boldsymbol{r})\Psi_{\boldsymbol{K},2}(-\boldsymbol{r}), \quad \text{(B13)}$$

where $v(\alpha)$ is the Fermi velocity. Also in the point $\boldsymbol{r}_0 = \frac{1}{3}(\boldsymbol{a}_1 - \boldsymbol{a}_2)$, the spinor component $\Psi_{\boldsymbol{K},2}(\boldsymbol{r}_0) = 0$ and the Fermi velocity reduces to

$$v(\alpha) = \Psi_{\boldsymbol{K},1}(\boldsymbol{r_0})\Psi_{\boldsymbol{K},1}(-\boldsymbol{r_0}). \quad \text{(B14)}$$

APPENDIX C: FRUSTRATION IN THE ELECTRONIC WAVE-FUNCTIONS OF GRAPHENE: EFFECTS OF THE UNDERLYING TRIGONAL SYMMETRY

Consider the case of graphene. Each sublattice, say A, is a 2D Bravais triangular lattice with lattice vectors,

$$\boldsymbol{a}_1 = \frac{a}{2}(\sqrt{3}, 3), \qquad \boldsymbol{a}_2 = \frac{a}{2}(-\sqrt{3}, 3), \quad \text{(C1)}$$

where $a = 1.42$ Å is the distance between C atoms. The B sublattice is obtained by a shift of the A sublattice by the basis vector $\boldsymbol{\delta}_1$. It is customary to define the following triad of vectors:

$$\boldsymbol{\delta}_1 = a(0, -1), \boldsymbol{\delta}_2 = \frac{a}{2}(-\sqrt{3}, 1), \quad \boldsymbol{\delta}_3 = \frac{a}{2}(\sqrt{3}, 1), \quad \text{(C2)}$$

that point out to the first neighbors and serve as a translation to obtain the other bipartite sublattice. Then,

$$\begin{aligned} \boldsymbol{a}_1 &= \boldsymbol{\delta}_3 - \boldsymbol{\delta}_1, \\ \boldsymbol{a}_2 &= \boldsymbol{\delta}_2 - \boldsymbol{\delta}_1, \\ \boldsymbol{a}_3 = \boldsymbol{a}_1 - \boldsymbol{a}_2 &= \boldsymbol{\delta}_3 - \boldsymbol{\delta}_2. \end{aligned} \quad \text{(C3)}$$

The trigonal lattice has the following reciprocal lattice vectors:

$$\boldsymbol{G}_1 = \frac{2\pi}{3a}(\sqrt{3}, 1), \qquad \boldsymbol{G}_2 = \frac{2\pi}{3a}(-\sqrt{3}, 1). \quad \text{(C4)}$$

Graphene's electronic properties are well described by a single-orbital tight-binding (TB) approximation,

$$\boldsymbol{H}_0 = -t_0 \sum_{\boldsymbol{r}_j}\sum_{n=1}^{3}\left[\hat{\psi}^\dagger(\boldsymbol{r}_j)\hat{\chi}(\boldsymbol{r}_j + \boldsymbol{\delta}_n) + \text{H.c.}\right], \quad \text{(C5)}$$

where $\boldsymbol{r}_j$ runs over all A sites of the Bravais lattice, and the hopping integral (also known as the transfer integral) $t_0 \approx 2.7$ eV. $\hat{\psi}^\dagger(\boldsymbol{r}_j)$ and $\hat{\chi}(\boldsymbol{r}_j + \boldsymbol{\delta}_n)$ are creation and annihilation electron operators on the A sublattice (at position $\boldsymbol{r}_j$) and the B sublattice (at position $\boldsymbol{r}_j + \boldsymbol{\delta}_n$), respectively.

One can reduce the Hamiltonian to a 2×2 matrix (because the lattice only contains two non-equivalent sites) by a Fourier transform:

$$\hat{\psi}^\dagger(\boldsymbol{r}_j) = \sum_{\boldsymbol{k}} \hat{\psi}^\dagger_{\boldsymbol{k}} e^{i\boldsymbol{k}\cdot\boldsymbol{r}_j} \tag{C6}$$

and

$$\hat{\chi}(\boldsymbol{r}_j + \boldsymbol{\delta}_n) = \sum_{\boldsymbol{k}} \hat{\chi}_{\boldsymbol{k}} e^{i\boldsymbol{k}\cdot(\boldsymbol{r}_j+\boldsymbol{\delta}_n)}. \tag{C7}$$

The Hamiltonian is written as an effective 2×2 Hamiltonian matrix $H(\boldsymbol{k})$ acting on a wave vector,

$$\boldsymbol{H}_0 = -t_0 \sum_{\boldsymbol{k}} (\psi^*_{\boldsymbol{k}}, \chi^*_{\boldsymbol{k}}) \begin{pmatrix} 0 & H_{AB}(\boldsymbol{k}) \\ H^*_{AB}(\boldsymbol{k}) & 0 \end{pmatrix} \begin{pmatrix} \psi_{\boldsymbol{k}} \\ \chi_{\boldsymbol{k}} \end{pmatrix}, \tag{C8}$$

where $H_{AB}(\boldsymbol{k}) = -t_0 f(\boldsymbol{k})$ and $f(\boldsymbol{k})$ with the following complex function:

$$f(\boldsymbol{k}) = \sum_{n=1}^{3} e^{-i\boldsymbol{k}\cdot\boldsymbol{\delta}_n}. \tag{C9}$$

The corresponding Schrödinger equation is

$$\begin{pmatrix} 0 & H_{AB}(\boldsymbol{k}) \\ H^*_{AB}(\boldsymbol{k}) & 0 \end{pmatrix} \begin{pmatrix} \psi_{\boldsymbol{k}} \\ \chi_{\boldsymbol{k}} \end{pmatrix} = E(\boldsymbol{k}) \begin{pmatrix} \psi_{\boldsymbol{k}} \\ \chi_{\boldsymbol{k}} \end{pmatrix}, \tag{C10}$$

Graphene's energy dispersion is found from Eq. (C10), from where $E(\boldsymbol{k}) = \pm t_0 |f(\boldsymbol{k})|$ with

$$|f(\boldsymbol{k})|^2 = \sum_{n,s=1}^{3} e^{i\boldsymbol{k}\cdot(\boldsymbol{\delta}_n - \boldsymbol{\delta}_s)} \tag{C11}$$

or using the relations Eq. (C3),

$$|f(\boldsymbol{k})|^2 = 3 + 2\cos(\boldsymbol{k}\cdot\boldsymbol{a}_1) + 2\cos(\boldsymbol{k}\cdot\boldsymbol{a}_2) + 2\cos(\boldsymbol{k}\cdot\boldsymbol{a}_3) \tag{C12}$$

where the energy dispersion is now given by the triangular lattice basis vectors. The eigenfunctions are thus

$$\Psi_{\boldsymbol{k}}(\boldsymbol{r}_j) \equiv \begin{pmatrix} \psi_{\boldsymbol{k}}(\boldsymbol{r}_j) \\ \chi_{\boldsymbol{k}}(\boldsymbol{r}_j + \boldsymbol{\delta}_1) \end{pmatrix} = \frac{e^{i\boldsymbol{k}\cdot\boldsymbol{r}_j}}{\sqrt{N}} \begin{pmatrix} 1 \\ \pm e^{-i\boldsymbol{k}\cdot\boldsymbol{\delta}_1} \end{pmatrix}. \tag{C13}$$

Observe how in the previous definition, we assign arbitrarily the vector δ_1 to a given A site. This avoid to carry a label for n in the left-hand side of the definition.

Now consider the squared Hamiltonian $\mathbf{H}_0^2$ obtained from Eq. (C8), its Schrödinger equation is

$$\begin{pmatrix} H^2_{AB}(\boldsymbol{k}) & 0 \\ 0 & H^2_{AB}(\boldsymbol{k}) \end{pmatrix} \begin{pmatrix} \psi_{\boldsymbol{k}} \\ \chi_{\boldsymbol{k}} \end{pmatrix} = E^2(\boldsymbol{k}) \begin{pmatrix} \psi_{\boldsymbol{k}} \\ \chi_{\boldsymbol{k}} \end{pmatrix}, \tag{C14}$$

implying that the components of the wavefunction on the A and B sublattices are decoupled. Thus $\mathbf{H}_0^2$ describes atoms in a triangular lattice as the squaring of H renormalizes one of the bipartite sublattices. The spectrum of $\mathbf{H}_0^2$ is obtaining by folding the original spectrum of $\mathbf{H}_0$ around $E = 0$. Obviously,

$$\mathbf{H}_0^2 = \begin{pmatrix} |f(\boldsymbol{k})|^2 & 0 \\ 0 & |f(\boldsymbol{k})|^2 \end{pmatrix}, \tag{C15}$$

which using Eq. (C12) completes our renormalization to a triangular lattice. We now remark that t_0 is squared in $\mathbf{H}_0^2$ and thus now antibonding and bonding states are map into the top of the band. This is seen by setting in Eq. (C12) $\boldsymbol{k}\cdot\boldsymbol{a}_1 = \boldsymbol{k}\cdot\boldsymbol{a}_2 = 0$ from where $\boldsymbol{k}\cdot\boldsymbol{a}_3 = 0$ resulting in $E^2(0) = 9t_0^2$ or $E(0) = \pm 3t_0$.

Let us find the ground state of Eq. (C15). A naive way is to perform a trial of the phases with the maximal phase difference, $\boldsymbol{k}\cdot\boldsymbol{a}_1 = \boldsymbol{k}\cdot\boldsymbol{a}_2 = \pi$, but now

$$\boldsymbol{k}\cdot\boldsymbol{a}_3 = \boldsymbol{k}\cdot(\boldsymbol{a}_1 - \boldsymbol{a}_2) = 0. \tag{C16}$$

The third bond is thus frustrated and increases the energy by 2, resulting in $E(k) = \pm t_0$. It turns out that this is exactly the energy where the Van-Hove singularities are found in graphene. These singularities are in fact similar to the confined states in the sense that are made form localized dimers, disconnected from the lattice by making zero such bonds. The degeneracy is given by the number of dimers. To lower the energy, the system needs to further reduce its frustration. As explained in the text, this leads to a depletion of the DOS. In disordered systems, such depletion leads to a Lifshitz tail. In graphene, this leads to the Dirac cone where the DOS goes linearly to zero towards $E \to 0$. Once graphene's periodicity is broken by adding impurities or by adding edges, confined zero energy modes appear at $E = 0$ and in fact is possible to count them; they are important for the magnetic properties of graphene [29,40].

To reach zero, we set $\boldsymbol{k}\cdot\boldsymbol{a}_1 = \phi, \boldsymbol{k}\cdot\boldsymbol{a}_2 = -\phi$ from where $\boldsymbol{k}\cdot\boldsymbol{a}_3 = 2\phi$. As $\cos\phi = \cos(-\phi) = -1/2$, we finally obtain $E(\boldsymbol{k}) = 0$. By working out the algebra, it turns out that this special wave vector is precisely the point $\boldsymbol{k} = \boldsymbol{K}$. By interchanging the sign of the phases, we get the other Dirac point $\boldsymbol{k} = \boldsymbol{K}'$. As for $E = 0$ states can be pseudo-spin-polarized, we end up concluding that our minimal frustrated state is fourfold degenerated.

Let us quantify the previous observations about frustration. First notice how Eq. (C11) depends upon phase differences between neighboring bonds, as we have from Eq. (C13),

$$g_{\boldsymbol{k}}(\boldsymbol{r}_j) = \pm\psi_{\boldsymbol{k}}(\boldsymbol{r}_j)\chi^*_{\boldsymbol{k}}(\boldsymbol{r}_j) = \pm\frac{e^{i\boldsymbol{k}\cdot\boldsymbol{\delta}_1}}{\sqrt{N}} \tag{C17}$$

where now we drop the vector $\boldsymbol{\delta}_1$ in $\chi^*_{\boldsymbol{k}}(\boldsymbol{r}_j + \boldsymbol{\delta}_1)$ as is clear that on each site in A we assign only one corresponding partner in B. Also, we drop the minus sign as this is irrelevant in the squared Hamiltonian. In such a form, we can perform a sum over all bonds and notice that

$$|f(\boldsymbol{k})|^2 = \frac{1}{2}\sum_{\boldsymbol{r}_j}\sum_{s=1}^{6} g^*_{\boldsymbol{k}}(\boldsymbol{r}_j) g_{\boldsymbol{k}}(\boldsymbol{r}_j + a_s) + 3 \tag{C18}$$

where a_s are the second neighbors in H_0 and first neighbors if using the triangular lattice corresponding to H_0^2, i.e., $\pm\boldsymbol{a}_1, \pm\boldsymbol{a}_2, \pm(\boldsymbol{a}_1 - \boldsymbol{a}_2)$, while the last term is the self-energy corresponding to the interaction of the phases at the same site. It follows that

$$E^2(\boldsymbol{k}) - 3t_0^2 = t_0^2 F(\boldsymbol{k}), \tag{C19}$$

where the sum of bonding (frustration) plus antibonding contribution is

$$F(\boldsymbol{k}) = \frac{1}{2}\sum_{\boldsymbol{r}_j}\sum_{s=1}^{6} g^*_{\boldsymbol{k}}(\boldsymbol{r}_j) g_{\boldsymbol{k}}(\boldsymbol{r}_j + a_s). \tag{C20}$$

The total contribution from frustration can be further obtained by subtracting the bonding limit, however, as is a constant, we leave $F(\boldsymbol{k})$ as a measure of frustration. The ground state $E = 0$ is obtained when the frustration and antibonding contributions balance the self-energy in such a way that $F(\boldsymbol{K}) = -3$, while the frustration is increased as we depart from the K point resulting in

$$F(\boldsymbol{k}) = 2\cos(\boldsymbol{k}\cdot\boldsymbol{a}_1) + 2\cos(\boldsymbol{k}\cdot\boldsymbol{a}_2) + 2\cos(\boldsymbol{k}\cdot\boldsymbol{a}_3). \quad \text{(C21)}$$

Obviously, this is the contribution from the six bonds in $\boldsymbol{H}_0^2$, however, the important point here is that the frustration is written in terms of the phase differences between neighbors.

How do we translate these ideas to a continuous low-energy model? The simplest way is to go into the lowest frustrated state and develop $F(\boldsymbol{k})$ in Eq. (C21) using $\boldsymbol{k} = \boldsymbol{K} + \boldsymbol{q}$ where $qa_0 << 1$. As expected,

$$F(\boldsymbol{k}) = F(\boldsymbol{K}) + (v_F/t_0)^2 q^2 \quad \text{(C22)}$$

from where is clear that the Fermi velocity indicates how fast the frustration is raising with q. Yet, we need to generalize this procedure to the twisted bilayer without knowing the energy dispersion.

We start by noticing that for the twisted bilayer, still we have the phases between neighbors, which are contained in $g_k(\boldsymbol{r}) = \psi_k(\boldsymbol{r})\chi_k^*(\boldsymbol{r})$ where the site index j was dropped as we deal with a continuous. Next we need to compare with the phases of the first-neighbors in the triangular lattice $g_k(\boldsymbol{r} + \bar{\boldsymbol{a}}_s)$. Here where we depart from the case of graphene as we can not use the Moiré vectors $\boldsymbol{a}_1, \boldsymbol{a}_2$ as neighbors as, for example, $\boldsymbol{r} + \boldsymbol{a}_1$ produces a site that is far away from a second neighbor. Therefore $\bar{\boldsymbol{a}}_s$ is used to denote a second neighbor. We develop in series and sum over neighbors, $g_k(\boldsymbol{r} + \bar{\boldsymbol{a}}_s)$ resulting in

$$F(\boldsymbol{k}) \approx \int_S d^2\boldsymbol{r} g_k^*(\boldsymbol{r})\left(g_k(\boldsymbol{r}) + \frac{1}{2}\sum_{s=1}^{6}\bar{\boldsymbol{a}}_s\cdot\nabla g_k(\boldsymbol{r})\right). \quad \text{(C23)}$$

Here, the gradient will produce a term proportional to q in the low energy version developed around $\boldsymbol{K}$, as observed in the spectrum [15].

[1] S. Nishijima, S. Eckroad, A. Marian, K. Choi, W. S. Kim, M. Terai, Z. Deng, J. Zheng, J. Wang, K. Umemoto, J. Du, P. Febvre, S. Keenan, O. Mukhanov, L. D. Cooley, C. P. Foley, W. V. Hassenzahl, and M. Izumi, Superconductivity and the environment: a Roadmap, Supercond. Sci. Technol. **26**, 113001 (2013).

[2] S. Kudo, T. Yoshida, S. Ideta, K. Takashima, H. Anzai, T. Fujita, Y. Nakashima, A. Ino, M. Arita, H. Namatame, M. Taniguchi, K. M. Kojima, S. Uchida, and A. Fujimori, Temperature evolution of correlation strength in the superconducting state of high-T_c cuprates, Phys. Rev. B **92**, 195135 (2015).

[3] B. Keimer, S. Kivelson, and M. E. A. Norman, From quantum matter to high-temperature superconductivity in copper oxides, Nature (London) **518**, 179186 (2015).

[4] T. Wang, N. F. Q. Yuan, and L. Fu, Moiré Surface States and Enhanced Superconductivity in Topological Insulators, Phys. Rev. X **11**, 021024 (2021).

[5] K. Yamazaki, M. Ochi, D. Ogura, K. Kuroki, H. Eisaki, S. Uchida, and H. Aoki, Superconducting mechanism for the cuprate $Ba_2Cu\,O_{3+\delta}$ based on a multiorbital Lieb lattice model, Phys. Rev. Research **2**, 033356 (2020).

[6] M.-S. Nam and A. Ardavan, Universal limiting transition temperature for the high T_c superconductors, arXiv:2010.00572.

[7] S. Tan, Y. Liu, Y. Mou, and S. Feng, Anisotropic dressing of electrons in electron-doped cuprate superconductors, Phys. Rev. B **103**, 014503 (2021).

[8] B. Kyung, D. Sénéchal, and A.-M. S. Tremblay, Pairing dynamics in strongly correlated superconductivity, Phys. Rev. B **80**, 205109 (2009).

[9] M. Capone, M. Fabrizio, C. Castellani, and E. Tosatti, Strongly correlated superconductivity, Science **296**, 2364 (2002).

[10] Y. Cao, V. Fatemi, S. Fang, K. Watanabe, T. Taniguchi, E. Kaxiras, and P. Jarillo-Herrero, Unconventional superconductivity in magic-angle graphene superlattices, Nature (London) **556**, 43 (2018).

[11] M. Yankowitz, S. Chen, H. Polshyn, Y. Zhang, K. Watanabe, T. Taniguchi, D. Graf, A. F. Young, and C. R. Dean, Tuning superconductivity in twisted bilayer graphene, Science **363**, 1059 (2019).

[12] A. Kerelsky, L. McGilly, and D. E. A. Kennes, Maximized electron interactions at the magic angle in twisted bilayer graphene, Nature (London) **572**, 95 (2019).

[13] R. Bistritzer and A. H. MacDonald, Moiré bands in twisted double-layer graphene, Proc. Natl. Acad. Sci. USA **108**, 12233 (2011).

[14] J. M. B. L. dos Santos, N. M. R. Peres, and A. H. Castro Neto, Graphene Bilayer With a Twist: Electronic Structure, Phys. Rev. Lett. **99**, 256802 (2007).

[15] G. Tarnopolsky, A. J. Kruchkov, and A. Vishwanath, Origin of Magic Angles in Twisted Bilayer Graphene, Phys. Rev. Lett. **122**, 106405 (2019).

[16] J. Wang, Y. Zheng, A. J. Millis, and J. Cano, Chiral approximation to twisted bilayer graphene: Exact intravalley inversion symmetry, nodal structure and implications for higher magic angles, Phys. Rev. Research **3**, 023155 (2021).

[17] F. K. Popov and A. Milekhin, Hidden wave function of twisted bilayer graphene: Flat band as a landau level, Phys. Rev. B **103**, 155150 (2021).

[18] K. Hejazi, C. Liu, and L. Balents, Landau levels in twisted bilayer graphene and semiclassical orbits, Phys. Rev. B **100**, 035115 (2019).

[19] A. Uri, S. Grover, Y. Cao, J. Â. A. Crosse, K. Bagani, D. Rodan-Legrain, Y. Myasoedov, K. Watanabe, T. Taniguchi, P. Moon, M. Koshino, P. Jarillo-Herrero, and E. Zeldov, Mapping the twist-angle disorder and Landau levels in magic-angle graphene, Nature (London) **581**, 47 (2020).

[20] X.-L. Qi and S.-C. Zhang, Topological insulators and superconductors, Rev. Mod. Phys. **83**, 1057 (2011).

[21] L. Zou, H. C. Po, A. Vishwanath, and T. Senthil, Band structure of twisted bilayer graphene: Emergent symmetries, commensu-

rate approximants, and Wannier obstructions, Phys. Rev. B **98**, 085435 (2018).
[22] C. Xu and L. Balents, Topological Superconductivity in Twisted Multilayer Graphene, Phys. Rev. Lett. **121**, 087001 (2018).
[23] M. Fidrysiak, M. Zegrodnik, and J. Spałek, Unconventional topological superconductivity and phase diagram for an effective two-orbital model as applied to twisted bilayer graphene, Phys. Rev. B **98**, 085436 (2018).
[24] Y.-Z. You and A. Vishwanath, Superconductivity from valley fluctuations and approximate SO(4) symmetry in a weak coupling theory of twisted bilayer graphene, npj Quantum Mater. **4**, 16 (2019).
[25] E. Khalaf, S. Chatterjee, N. Bultinck, M. P. Zaletel, and A. Vishwanath, Charged Skyrmions and topological origin of superconductivity in magic angle graphene, Sci. Adv. **7**, eabf5299 (2021).
[26] M. Rodriguez-Vega, M. Vogl, and G. A. Fiete, Floquet engineering of twisted double bilayer graphene, Phys. Rev. Research **2**, 033494 (2020).
[27] J. Kang and O. Vafek, Non-abelian dirac node braiding and near-degeneracy of correlated phases at odd integer filling in magic-angle twisted bilayer graphene, Phys. Rev. B **102**, 035161 (2020).
[28] P. San-Jose, J. Gonzalez, and F. Guinea, Non-Abelian Gauge Potentials in Graphene Bilayers, Phys. Rev. Lett. **108**, 216802 (2012).
[29] G. G. Naumis, Internal mobility edge in doped graphene: Frustration in a renormalized lattice, Phys. Rev. B **76**, 153403 (2007).
[30] J. E. Barrios-Vargas and G. G. Naumis, Doped graphene: the interplay between localization and frustration due to the underlying triangular symmetry, J. Phys.: Condens. Matter **23**, 375501 (2011).
[31] M. C. Fumiko Yonezawa, Theory of electronic properties of amorphous semiconductors, in *Fundamental Physics of Amorphous Semiconductors: Proceedings of the Kyoto Summer Institute Kyoto, Japan, September 811, 1980*, 1st ed., edited by F. Y. Fumiko Yonezawa, Springer Series in Solid-State Sciences Vol. 46 (Springer-Verlag, Berlin, Heidelberg, 1981), pp. 119–144.
[32] M. Cohen, Topology, geometry, elementary excitations and physical properties of disordered materials, in *Topological Disorder in Condensed Matter*, 1st ed., edited by F. Y. Hellmut Fritzsche, Springer Series in Solid-State Sciences Vol. 25, (Springer-Verlag, Berlin, Heidelberg, 1983), pp. 122–141.
[33] L. A. Gonzalez-Arraga, J. L. Lado, F. Guinea, and P. San-Jose, Electrically Controllable Magnetism in Twisted Bilayer Graphene, Phys. Rev. Lett. **119**, 107201 (2017).
[34] H.K. Pal, S. Spitz, and M. Kindermann, Emergent Geometric Frustration and Flat Band in Moiré Bilayer Graphene, Phys. Rev. Lett. **123**, 186402 (2019).
[35] M. Kohmoto and B. Sutherland, Electronic States on a Penrose Lattice, Phys. Rev. Lett. **56**, 2740 (1986).
[36] M. Arai, T. Tokihiro, T. Fujiwara, and M. Kohmoto, Strictly localized states on a two-dimensional penrose lattice, Phys. Rev. B **38**, 1621 (1988).
[37] G. G. Naumis, R. A. Barrio, and C. Wang, Effects of frustration and localization of states in the penrose lattice, Phys. Rev. B **50**, 9834 (1994).
[38] S. Kirkpatrick and T. P. Eggarter, Localized states of a binary alloy, Phys. Rev. B **6**, 3598 (1972).
[39] G. G. Naumis, C. Wang, and R. A. Barrio, Frustration effects on the electronic density of states of a random binary alloy, Phys. Rev. B **65**, 134203 (2002).
[40] J. Barrios-Vargas and G. G. Naumis, Pseudo-gap opening and dirac point confined states in doped graphene, Solid State Commun. **162**, 23 (2013).
[41] V. H. Nguyen, D. Paszko, M. Lamparski, B. Van Troeye, V. Meunier, and J.-C. Charlier, Electronic localization in small-angle twisted bilayer graphene, 2D Materials **8**, 035046 (2021).
[42] J. C. Phillips, Topology of covalent non-crystalline solids i: Short-range order in chalcogenide alloys, J. Non-Cryst. Solids **34**, 153 (1979).
[43] C. L. Kane and T. C. Lubensky, Topological boundary modes in isostatic lattices, Nat. Phys. **10**, 39 (2014).
[44] A. Huerta and G. Naumis, Relationship between glass transition and rigidity in a binary associative fluid, Phys. Lett. A **299**, 660 (2002).
[45] A. Huerta and G. G. Naumis, Evidence of a glass transition induced by rigidity self-organization in a network-forming fluid, Phys. Rev. B **66**, 184204 (2002).
[46] H. M. Flores-Ruiz, G. G. Naumis, and J. C. Phillips, Heating through the glass transition: A rigidity approach to the boson peak, Phys. Rev. B **82**, 214201 (2010).
[47] H. M. Flores-Ruiz and G. G. Naumis, Boson peak as a consequence of rigidity: A perturbation theory approach, Phys. Rev. B **83**, 184204 (2011).